Extraction of heavy-flavor transport coefficients in QCD matter

EMMI RRTF

December 13, 2016

Abstract

Systematic investigation of the modeling components for open heavy-flavor diffusion and energy loss in strongly interacting matter in their application to heavy-flavor observables in high-energy heavy-ion collisions. Develop procedures for error assessments and arrive at quantitative estimates for the (low-momentum) heavy-flavor diffusion coefficient as a long-wavelength characteristic of QCD matter as function of temperature, and for energy loss coefficients of high-momentum heavy-flavor particles.

Contents

1 Introduction

The characterization of the properties of matter can be carried out at various levels, based on different ways of testing its repsonse to external excitations. Bulk properties are encoded in the equation of state, $\epsilon(P)$, which characterizes how a system responds to changes in its pressure. Transport coefficients, on the other hand, charaterize how small perturbations from equilibrium (often associated with conserved quantities), are transmitted through the medium. In quantum field theory, transport coefficients can be formulated as the zero-energy and long-wavelength limit of correlation functions. This, in particular, allows to establish connections between microscopic calculations of spectral (or correlation) functions and their undelying transport coefficients.

High-energy collisions of atomic nuclei have revealed remarkable properties of strongly interactinig matter at high temperature. For example, the ratio of shear viscosity to the entropy density, η/s, of the medium has been inferred to be the smallest of any known substance. However, the extraction of this quantity, including its temperature dependence, from fitting viscous hydrodynamic simluation of the fireball to final-state hadron spectra, is rather indirect, involving the entire sytem evolution. Progress has been made in controlling basic features of the fireball evolution [1], but significant uncertainties persist, *e.g.*, in the initial conditions and pre-equilibrium evolution. Furthermore, the microscopic origin of the small η/s, *i.e.*, how it emerges from the fundamental interactions in the medium, remains a burning question that calls for additional observables and methods. In particular, non-montonuous features of transport coefficients in the vicinity fo the (pseudo-) critical transition temperature are of fundamental relevance to understanding the phase structure of Qunatum Chromodynamics (QCD).

The diffusion of heavy quarks in QCD matter at not too high temperatures has long been recognized as a promising concept and phenomenological tool to diagnose the medium produced in heavy-ion collisions (HICs) [2]. The basic realization is that the heavy-quark (HQ) mass, m_Q, is parametrically large compared to the important scales that characterize the QCD medium produced in experiment, *i.e.*, its typical temperature, but also relative to the more fundamental quantities such as the QCD scale parameter, $\Lambda_{\rm QCD}$, the light-quark masses, and the pseudo-critical transition temperature, $T_{\rm pc}$. This implies a sequence of benefits, both phenomenologically and theoretically, namely that (a) the production of heavy quarks is reasonably well controlled as a hard initial-state process, (b) their subsequent motion through the medium is, at low momenta, of a diffusive "Brownian" type and thus characterized by well-defined transport coefficients, most notably the spatial diffusion coefficient $\mathcal{D}_s$, (c) their "identitiy" is preserved in the hadronization process thus providing tests of the latter's nature, (d) their interactions with the medium are of potential-type *i.e.*, elastic collisions with small energy transfer. Furthermore, the thermalization time of heavy quarks is delayed relative to the light partons of the bulk medium, parametrically by a factor of order $\sim M_Q/T$, which renders it comparable to the lifetime of the QGP fireballs in HICs. Thus, heavy-flavor (HF) particles are not expected to fully thermalize and in this way preserve a memory of their interaction history which can serve as a gauge of their interaction strength with the medium. The (low-momentum) HF diffusion coefficient, $\mathcal{D}_s$, arguably provides the most direct window on the in-medium QCD force in HICs, and thus on the coupling strength of the medium. To the extent that the same in-medium interactions are operative in the transport of different quantities, *e.g.*, energy-momentum or electric charge, one expects the pertinent transport coefficients to be closely related when scaled to dimensionless units, *e.g.*, $\eta/s \sim \mathcal{D}_s(2\pi T) \sim \sigma_{\rm EM}/T$ (where $\sigma_{\rm EM}$ denotes the electric conductivity).

Over the last decade, open HF observables, *i.e.*, transverse-momentum (p_T) spectra and elliptic flow (v_2) of particles containing a single charm (c) or bottom (b) quark (or their decay products), have much advanced and are now at the verge of becoming a precision probe of QCD matter. This has triggered an intense theoretical activity aimed at understanding the intriguing experimental results on how HF spectra are modified when going from elementary proton-proton collision to reactions with incoming heavy nuclei, see, *e.g.*, Refs. [3, 4, 5] for recent reviews. The modeling efforts have now reached a critical stage. While several approaches have accomplished a qualitative or even semi-quantiative agreement with (some of the) existing data, it seems fair to say that there no single approach is yet able to quantitatively describe all available HF (mostly charm) measurements from the Relativistic Heavy-Ion Collider (RHIC) and the Large Hadron Collider (LHC), from low to high p_T. At the same time, a fundamental understanding of the underlying processes employed in the phenomenological modeling efforts requires the latter to be firmaly rooted in QCD. The complexity of the problem likely requires different prevalent mechanisms not only as a function of p_T (*e.g.*, collisional vs. radiative and/or perturbative vs. non-perturbative interactions) but also as a function of temperature. In addition, the accuracy of the information extracted from HF observables will also hinge on a realistic space-time evolution for the background medium, *e.g.*, hydrodynamic or transport models, as well as initial conditions for the HQ spectra, possibly modified by "cold-nuclear-matter" (CNM) effects in the incoming nuclei prior to the collision. Indeed, the individual models are based on rather different ingredients for the different components, including a varying degree of fit parameters (*e.g.*, K factors for the transport coefficients). At this point, it becomes compelling to go beyond incremental improvements of individual appraoches and thus launch a broadly vetted effort by the active members of the community becomes mandatory. For this purpose an EMMI Rapid Reaction Task Force was initiated and formed, and an initial meeting convened at GSI Darmstadt (Gemrany) in July 2016 [6]. The key open questions and objectives in the open HF problem that were identified and addressed during the meeting are:

1) How do the conceptual underpinnings of the current theoretical models compare and constrain their applicability in various regions of phase space and temperature? Do these uncertainties provide a suffcient (and consistent) basis for systematic uncertainty evaluations of the extracted transport coeffcients? How can quantitative connections to the jet quenching in the light-flavor sector be made?

2) What is the impact of the available implementations of hadronization, in particular heavy-quark coalescence, on D-meson spectra, and how can they be seamlessly connected to the QGP and hadronic diffusion processes?

3) What are the pros and cons for Boltzmann vs. Langevin implementations of the heavy-flavor transport in an evolving medium?

4) What is the role of the different medium evolution models, and how do different predictions for the temperature- and momentum-dependent transport coeffcients in current model calculations manifest themselves in comparison to existing data?

5) What are future precision requirements on existing observables, and are there other ways to look at the data (new observables) to improve current accuracies, and to what extent? In particular,

in what ways are the upcoming data at RHIC and the LHC crucial in extending our knowledge of heavy-quark phenomena in deconfined matter?

The present document is a first step in these directions by scrutinizing the different components in the modeling efforts and performing targeted calculcations by all involved parties to unravel, and ultimately quantify, how pertinent uncertainties impact the extraction of HF transport coefficients. It is organized as follows. In Sec. 2 we investigate the impact of the bulk evolution models, by evaluating their outcomes with a uniform transport coefficient, by comparing hydrodynamic simulations to coarse-graining techniques of microscopic transport models, and by adopting a common hydrodynamic framework with different HF transport coefficients. In Sec. 3 we study the differences in the treatment of HQ hadronization, in particular different schemes of HQ recombination with light partons in the quark-hadron transition of the bulk medium, as well as fragmentation mechanisms. In Sec. 4 the transport coefficients and HQ interactions as used by the different groups are scrutinized, specifically in the low- and high-p_T regimes, the role of the (in-medium) quark mass is addressed, and a publicly accessible repository of transport coefficients [7] is generated along with a pertinent applicability chart in momentum and temperature. In Sec. 5 the merits and caveats of different implementations of HF transport into bulk evolution models is discussed, specifically the Fokker-Planck/Langevin and the Boltzmann approach, as well as the problem of non-locality in radiative processes. In Sec. 6, a common baseline for the initial HQ spectra from pp collisions is developed along with a standardized implementation of CNM effcts. A summary with an outlook for future developments is given in Sec. 7.

2 Bulk Evolution Models

2.1 Results with Common Transport Coefficient

As an initial test of how different bulk medium evolution models as employed by the various research groups affect the results for HF observables, calculations were carried out by the groups using their evolution model but with a common pre-defined transport coefficient (for Langevin approaches) or pertinent cross section (for Boltzmann approaches). Specifically, pQCD Born diagrams for elastic charm-quark scattering off thermal quarks, anti-quarks and gluons were usedi, where, for example, the basic matrix element of t-channel gluon exchange is ggiven by

$$\mathcal{M}_t \propto \frac{\alpha_s}{t - m_D^2} \ . \tag{1}$$

The coupling constant has been fixed at $\alpha_s = 0.4$ (corresponding to g=2.24), the Debye mass at $m_D = gT$, and thermal parton masses in the heat bath at $m_{\rm th} = gT$ (assuming 3 massless quark flavors). For the charm-quark mass a constant value of $m_{\rm c}$=1.5 GeV has been used, and an overall K factor of 5 was applied to the squared matrix elements (numerical tables for the pertinent HQ transport coefficients are available from the HF-RRTF repository [7]). The resulting spatial HQ diffusion coefficient amounts to $\mathcal{D}_s(2\pi T) \simeq 6$ at T=300 MeV, with a weak temperature dependence. Furthermore, in the Langevin approaches, a uniform implementation of the Einstein relation was adopted, with friction (A) and transverse diffusion (B_0) coefficients as calculated from the pQCD scattering matrix elements and the longitudinal one adjusted to $B_1 = TEA$ to ensure the correct equilibrium limit ($E = \sqrt{m_c^2 + p^2}$ is the on-shell c-quark energy).

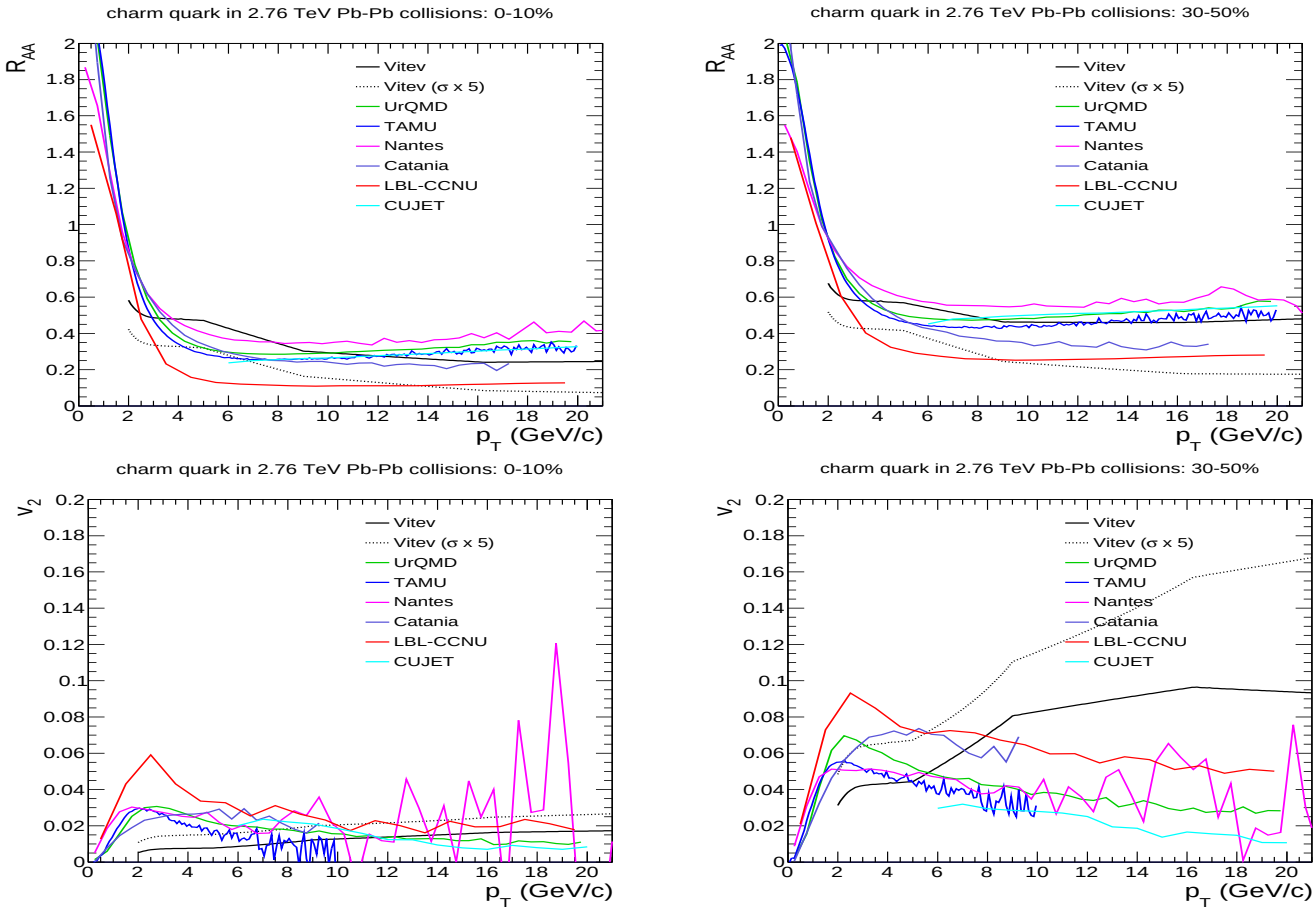

Figure 1: Comparison of the nuclear modification factor (upper panels) and elliptic flow (lower panels) of charm quarks in 0-10% (left panels) and 30-50% (right panels) Pb-Pb(2.76 TeV) collisions using a unique charm-quark transport coefficient for diffusion with the QGP phase in these reactions.

The charm-quark R_{AA} and v_2 were then computed at the end of QGP phase for 0-10% and 30-50% Pb-Pb(2.76TeV) collisions with the existing evolution models, restricted to the QGP evolution, and with initial charm-quark spectra from pp collisions without any CNM effects (such as shadowing or Cronin effect). The results are collected in Fig. 1. The $R_{\rm AA}$'s are reasonably well collimated in the fall-off region around $p_t \simeq 2\,$GeV. However, this essenetially enforced by charm-quark number conservation, as the total yield is essentially concentrated around this value. Below and above this p_t value a significant spread arises, both in the way the p_t=0 limit is approached and in the value around which the high-p_t $R_{\rm AA}$'s level off. For example, around $p_t \simeq 20\,$GeV, the latter vary from 0.15(0.3) for the LBNL transport model (slightly lower still in the energy-loss model of Vitev et al. with factor-5 upscaled cross sections and using a Bjorken expansion)up to about 0.4(0.6) in the Nantes model for (semi-) central collisions. On the other hand, the Catania, Nantes, TAMU and UrQMD (as well as the baslein Vitev moet al. model) are within a ragnge of 0.1 for most of the high-p_t range, while for low p_t Catania, TAMU and UrQMD seem to agree reasonably well. For the v_2 a somewhat similar picture emerges, with Nantes, TAMU and UrQMD agreeing quite well, Catania being slightly higher for central collisions, while Catania and LBNL are significantly higher for semi-central collisions.

To better understand the discrepancies and agreement, it is instructive to scrutinize the radial and elliptic flow of the underlying bulk medium evolutions.

2.2 Coarse-Graining of Transport Bulk Evolution

[Catania, PHSD, BAMPS]: local energy density, $\varepsilon(\vec{r})$, and cell velocity, $\vec{v}(\vec{r})$;
compare results to various hydrodynamic evolutions

2.3 Standard Hydrodynamic Model

[**DRAFT: S. Cao**];
Adopt, *e.g.*, from HQ-jet working group **[S.Cao(?)]** and/or OSU viscous EbyE which is publicly available;
Implement various transport coefficients to test momentum and temperature dependencies;
could envisage "best fit" procedure within a given microscopic model, but importance of tunable hydro input to map out hydro-input uncertainty (*e.g.*, initial flow, initial profile).

2.4 Bulk Comparisons

compare $\varepsilon(\vec{r})$, $\vec{v}(\vec{r})$ from coarse-grained transport with various hydro evolutions, including temperature [use lattice EoS]

3 Hadronization

The hadronization mechanism of heavy quarks into heavy mesons and baryons [8, 9] in heavy-ion collisions has been established as an important ingredient to the phenomenology of the observed heavy-flavor $R_{\rm AA}$ and v_2 at both RHIC [33, 34] and the LHC [35, 10]. As such it is critical to scrutinize the different theoretical treatments of this modeling component. In the following section (3.1) we first compare the impact of the various hadronization mechanisms from the literature as applied in current model approaches to the charm-quark spectra in Pb-Pb(2.76 TeV) collisions as computed with a common transport coefficient in Sec. 2.1. We then elaborate on different ways of implementing heavy-light quark coalesence by directly comparing several available approaches applied to the same input charm-quark spectrum within the same bulk medium background (temperature and flow field) and critically inspecting the effects on the resulting D-meson p_t spectra and v_2 in Sec. 3.2). Finally we discuss an alternative for in-medium hadronization based on a fragmentation scheme with surrounding medium partons in Sec. 3.3).

3.1 Comparison of Hadronization on Spectra from Common Transport Coefficients

3.2 Recombination in Thermal Medium

Traditionally, coalesence processes in heavy-ion collisions have been modeled in 3-momentum space amounting to an instantaneous approximation. This, in particular, allowed for a successful description of the hadron-v_2 and the baryon-over-meson ratio in the light and strange-quark sector in the intermediate-p_t region at RHIC. However, this approximation does not conserve energy in the 2$\rightarrow$1 hadron formation process and thus cannot recover the correct equilibrium limit. In Ref. [36] a resonance recombination model (RRM) has been developed using resonant quark-anti-quark scattering within a Boltzmann equation, which remedies both energy conservation and the equilibrium limit.

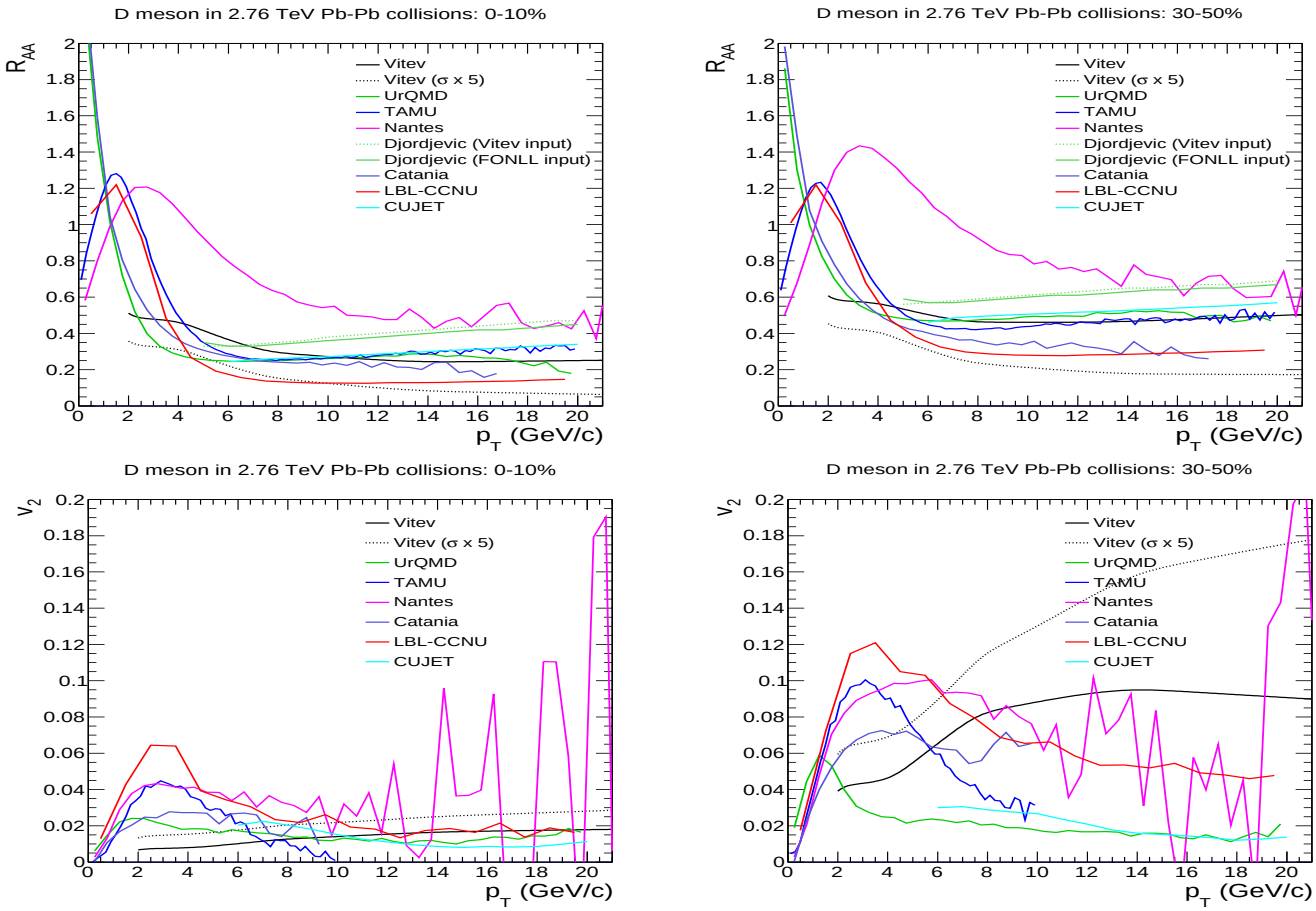

Figure 2: Comparison of the nuclear modification factor (upper panels) and elliptic flow (lower panels) of D-meson right after the hadronization transition, as obtained from the c-quark spectra obtained in the different evolution models with a common transport coefficient, displayed in Fig. 1, for 0-10% (left panels) and 30-50% (right panels) Pb-Pb(2.76 TeV) collisions.

It has been implemented in the heavy-quark context on a hydrodynamic hypersurface in Ref. [37]. In Fig. 3 we compare the results of these two coalescence appraoches when applying them to the c-quark spectra computed in Sec. 2.1 at the end of the QGP phase (within the TAMU hydro model). The resulting D-meson v_2 turns out to be surprisingly similar, while the p_t spectra within the RRM framework are significantly softer than within the instantaneous approximation. This is probably a consequence of the correct equilibrium limit within RRM, which *softens* the high-p_t spectra as to approach the thermal limit, while in the instantaneous approximation, the collinearity of the coalescing quarks tends to add 3-momentum in the conversion from c quarks to D mesons.

investigate dependence on heavy- and light-quark masses;

3.3 Fragmentation

[**DRAFT: A. Beraudo**];
investigate uncertainty of FFs;

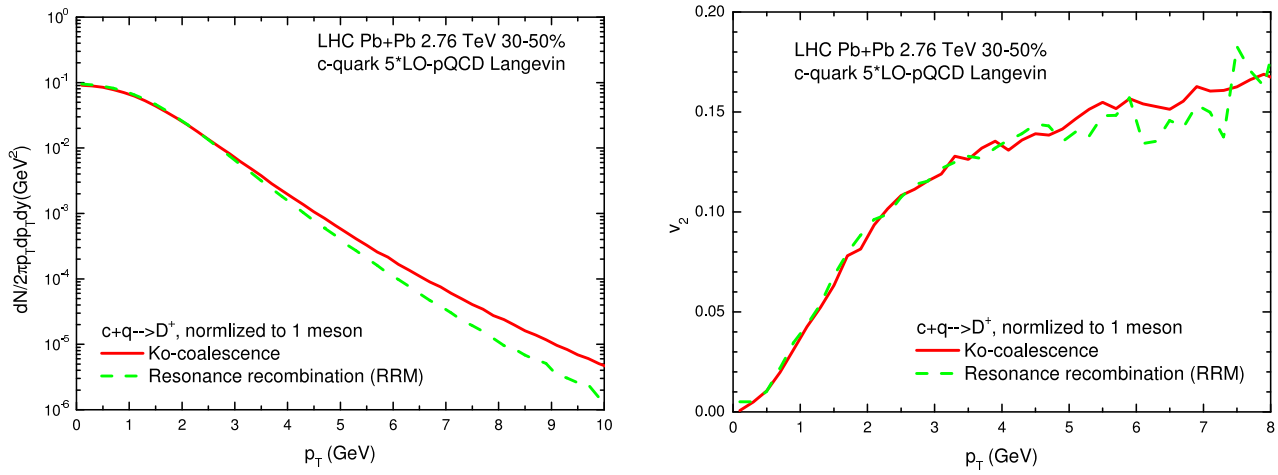

Figure 3: Comparison of the D-meson p_t spectra (left panel) and elliptic flow (right panel) produced through recombination processes at a critical temperature of $T_{\rm pc}$=170 MeV when using the resonance recombination model (RRM, dashed lines) [36, 37] and an instantaneous coalescence model (solid lines) [38] in 30-50% Pb-Pb(2.76 TeV) collisions. The input charm-quark spectra are taken from the Langevin simulations with the factor-5 upscaled pQCD interactions (using the TAMU hydro evolution) discussed in Sec. 2.1.

4 Transport Coefficients

4.1 General Features

(*some parts of this will be addressed in the introduction*)
emphasize and exploit benefits of HQ mass (HQET, lQCD); how to make use of the constraints provided by these frameworks; RG methods
rigorous defintion of transport coefficient $\mathcal{D}_s$ (via conserved current) in low-momentum limit as long-wavelength property of the medium; relation to η/s etc.;
3-momentum dependence of interactions [Soto, Escobedo, spatial lQCD correlators]

4.2 Comparison of Existing Models

plot compilations of A, B_0, B_1

4.3 Information and Constraints from Lattice QCD

QCD calculations can contribute to understanding of heavy flavor production in hot medium in several different ways. Lattice QCD cab provide some information on the heavy quark diffusion constant. These calculations can be compared to the calculations based on weak coupling expansion, which are valid are sufficiently high temperature. Diagonal and off-diagonal charm susceptibilities can provide information on the charm degrees of freedom across the QCD transition. Finally, spatial and temporal correlators provide information on in-medium properties of charm hadrons and or about their dissolution in hot medium. Below we will discuss the status of these calculations in more detail.

4.3.1 Heavy-quark diffusion constant

The spatial heavy quark diffusion constant can be defined in terms of spectral functions corresponding to current current correlators of heavy quarks

$$\sigma(\omega,\vec{p}) = \frac{1}{\pi}\int dt e^{i\omega t}\int d^3x e^{i\vec{x}\cdot\vec{p}}\langle[J_i(t,\vec{x}),J_i(0,0)]\rangle, \tag{2}$$

where $J_i = \bar{\psi}_h\gamma_i\psi$ with ψ_h being the heavy quark field. The spatial diffusion constant is defined as

$$\mathcal{D}_s = \lim_{\omega\to 0}\sigma(\omega,\vec{p}=0)/(\omega\chi_q\pi). \tag{3}$$

Here χ_q is the quark number susceptibility for heavy quarks. In the case of a large quark mass, $M \gg T$, the structure of the spectral function has a simple form for $\vec{p}=0$:

$$\sigma(\omega,0) = \frac{1}{\pi}\chi_q\frac{\omega\eta}{\omega^2+\eta^2}\frac{T}{M}, \tag{4}$$

where $\eta = T/(M\mathcal{D}_s)$ is drag coefficient entering the Langevin equation [13]. In other words, for zero spatial momentum the spectral function has a transport peak at $\omega \simeq 0$. For $p \ll T$ the structure of the spectral function can be worked out and it is determined by the same constant η [13], *i.e.*, for small momenta there is no dependence of the drag coefficient on the momentum. As one can see from Eq. (4) the width of the transport peak is very small for large quark mass. This makes the lattice determination of the heavy-quark diffusion coefficient very challenging [13, 11]. However, the difficulty associated with the large quark mass can be turned into an advantage. Namely, one can integrate out the heavy-quark degrees of freedom in the spirit of heavy-quark effective theory and reduce the current-current correlator to the correlator of the chromo-electric field strength [14]. The corresponding spectral function in the $\omega \to 0$ limit gives the momentum diffusion coefficient $\kappa = 2MT\eta$ [14]. Furthermore, this spectral function does not have a peak around $\omega = 0$, instead the high-ω and the low-ω regions are smoothly connected [14, 19]. From the point of view of reconstructing the spectral function from the lattice data this has a clear advantage since for determination of κ one has to determine the intercept rather than the width of the transport peak, and therefore the lattice determination of κ may be more easily feasible. Lattice determinations of κ in quenched QCD have been reported in Refs. [15, 17]. A prerequisite for the determination of the transport coefficient κ is sufficiently accurate data for the electric field strength correlator. Due to gluonic nature of the correlation functions the lattice data are very noisy and the use of noise reduction techniques is mandatory [15, 17]. In addition one has to perform calculations at several lattice spacings and perform a continuum extrapolation. This step has so far been performed only in Ref. [17]. Given the lattice data one relies on a fit ansatz that smoothly connects the known high-ω asymptotics of the spectral function with the form $\kappa\omega$ for small ω. This ansatz is not unique and the use of different ansätze translates into systematic errors in the determination of κ. The detailed analysis of Ref. [17] results in a value of

$$\kappa/T^3 = 1.8 - 3.4. \tag{5}$$

for $T = 1.5\,T_c$ (where $T_c \simeq 270\,\mathrm{MeV}$ for quenched QCD). This corresponds to a range of values for $\mathcal{D}_sT$ of 0.59-1.1. This result agrees with findings presented in Ref. [15] at fixed lattice spacing within errors.

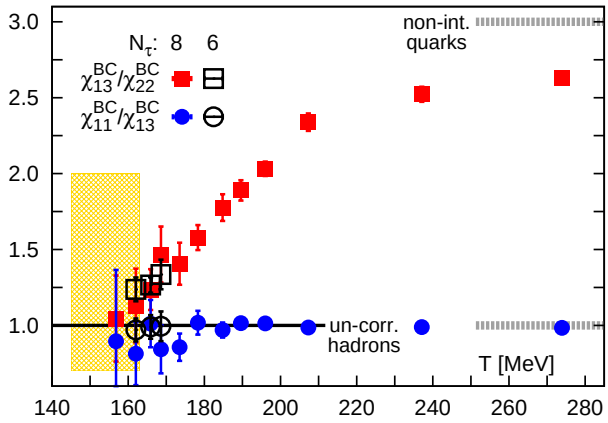

Figure 4: Ratio of baryon number charm correlations as functions of temperatures. The horizontal lines correspond to HRG and to quark gas. The ratio of correlations involving the same number of derivatives in baryon chemical potential but same number of derivatives with respect to charm chemical potential are always one because sectors with $|C| = 2, 3$ do not contribute because of the large charm quark mass [23].

Attempts to determine the spatial heavy-quark diffusion constant from current-current correlators have been presented in Ref. [16] in quenched QCD:

$$2\pi T\mathcal{D}_s = 1.8 \pm 0.5(stat.)^{+1.3}_{-0.5}(syst.), T = 1.46T_c. \tag{6}$$

This is significantly smaller than the value of $\mathcal{D}_s$ reported above. Note, however, that not all systematics effects have been taken into account in this analysis. As discussed before it is difficult to determine reliably the width of the transport peak.

For phenomenological applications it would be important to perform calculations in full QCD. With the current technology this is not possible since the noise reduction techniques are only available for quenched QCD. One possible way to deal with noise in full QCD would be to use a gradient-flow method.

The formulation of the heavy quark diffusion in terms of electric field strength correlators, or equivalently in terms of force-force correlators acting on the heavy quark turned out to be very useful when calculating the momentum diffusion coefficient in weak coupling expansion [20] or in AdS/CFT [18]. The value of κ from the lattice calculation given by Eq. (5) in fact agrees with the next-to-leading order weak coupling result of Ref. [20] if the value of $\alpha_s \simeq 0.26$ is used, although the perturbative series is badly convergent at even smaller values of the coupling.

4.3.2 Charm fluctuations and correlations and charm degrees of freedom in hot matter

Derivatives of the QCD pressure with respect to chemical potential

$$\chi^X_n = T^n \frac{\partial^n (p(T,\mu_X,\mu_Y)/T^4)}{\partial \mu^n_X} \chi^{XY}_{nm} = T^{n+m} \frac{\partial^{n+m} (p(T,\mu_X,\mu_Y)/T^4)}{\partial \mu^n_X \partial \mu^m_Y} \tag{7}$$

define fluctuations of conserved charge X or correlations between conserved charge X and conserved charge Y. These have been calculated on the lattice including the case of charm $X = C$ [23]. Fluctuations and correlation of conserved charges are sensitive to deconfinement and provide information on

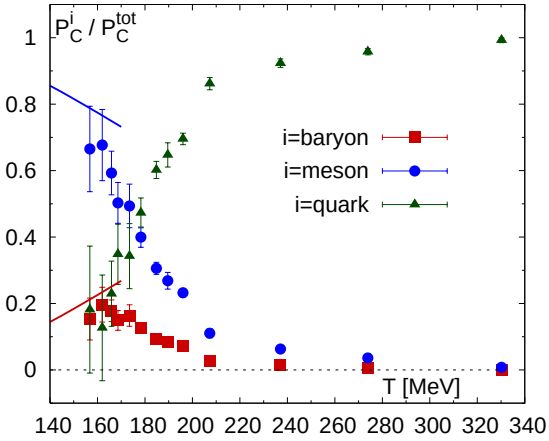

Figure 5: The partial pressure of charm quark, charm mesons and charm baryons normalized by the total charm pressure as function of the temperature [21].

the relevant degrees of freedom. At low temperature the fluctuations and correlations can be understood in terms of hadron resonance gas (HRG) model [25, 27, 23], while at high temperatures they can be understood in terms of quark degrees of freedom [28, 26, 23, 24]. This is demonstrated in Fig. 4 in terms of baryon number charm correlations. In fact these correlations together with charm fluctuations χ_2^C can clarify the nature of charm degrees of freedom. Below T_c charm fluctuations and correlations can be described in terms of HRG (c.f. Fig. 4). Above T_c the partial pressure of the charm degrees of freedom can be written as sum of partial pressures of charm mesons, charm baryons and charm quraks [21]. Using lattice data on χ_2^C, χ_{22}^{BC} and χ_{13}^{BC} one can obtain the partial pressures of charm quark, $p_q(T)$, partial pressure of charm mesons, $p_M(T)$ and partial pressure of charm baryons, $p_B(T)$, which are shown in Fig. 5. At T_c the partial baryon and meson pressures agree with HRG prediction, while the partial charm quark pressure is consistent with zero within errors. As the temperature increases the partial meson pressure and baryon pressure decrease and become very small for $T > 200$ MeV. This can be interpreted as gradual melting of charm hadrons above T_c. The important point here, however, is that hadron like excitations in the open charm sector may exist above T_c. Quarks dominate the charm pressure only for $T > 200$ MeV. At these temperatures charm quark properties, like in-medium mass and width can be extracted from charm fluctuations, χ_2^C, see Ref. [12]. As shown there the quasi-particle model with T-dependent effective charm quark mass works well [12].

4.3.3 Charm meson correlators

Properties of charm hadrons are encoded in the spectral functions. Temporal and spatial correlators that can be calculated in lattice QCD are related to the spectral functions. The temporal correlators are simple periodic Laplace transformation of the spectral functions. Therefore, many attempts to reconstruct the spectral functions by using Bayesian approach have been presented in the literature, mostly focusing on hidden heavy-flavor mesons (see, e.g., Ref. [30]). Unfortunately, there no studies available for the open heavy flavor hadrons so far. There is also another problem. Due to the fact the the temporal meson correlators are define only for Euclidean time separation $\tau < 1/(2T)$ there is a limited sensitivity to the in-medium modification of the spectral functions [11, 31, 32].

One can consider spatial meson correlation functions, which are much more sensitive to the in-medium modifications of the spectral functions [22]. However, the relation of the spatial meson correlators to the spectral functions is more complicated. It is given by double integral transformation [22]. Nevertheless, some qualitative information on the in-medium modifications of the open charm mesons can be obtained. It turns out that open charm meson spectral functions are modified already below T_c [22]. The in-medium modifications are large above T_c and for $T > 250$ MeV the spatial meson correlators are compatible with the propagation of un-correlated quark anti-quark pair, i.e. with dissolution of meson states. This is consistent with the findings of the previous section based on baryon charm correlations.

In the future it would be interesting to study temporal open heavy flavor meson correlators. It is interesting to note the modification of the open charm meson spectral functions below T_c are consistent with the modification of the baryon masses found in Ref. [29].

4.4 Repository of Fokker-Planck Coefficients

A, B_0, B_1 as function of T (160 - 600, step 20 MeV), p (0 - 40, step 0.2 GeV/c) **[CATANIA, NANTES, TAMU, TORINO, CCNU, FRANKFURT]**;
online repository generated and maintained by **[A.Andronic,R.Averbeck,S.Masciocchi]**

4.5 High-p_T Energy Loss and $\hat{q}$

[**DRAFT: I. Vitev + M. Djordjevic**];
α_s at vertices (running or not)? (GLV, SCT) for $\mathrm{d}\sigma^{2\to2}/\mathrm{d}q_T^2(E,T,q_T^2)$ and $\Delta E(L,E,T)$; deduce pertinent $\hat{q}$ **[All(!) Groups]**;
role of m_g^{th} in radiation

4.5.1 In-medium parton showers and heavy flavor

In the past several years new theoretical developments in the description of hard probes in heavy-ion collisions were enabled by the introduction of an effective theory of jet propagation in matter, Soft Collinear Effective Theory with Glauber Gluons, SCET$_{\rm G}$ [39, 40]. The collinear in-medium splitting functions, the building blocks in parton shower formation [41, 42], were obtained to first order in opacity. This allows for a unified description of vacuum and medium-induced branching. Applications so far, beyond the traditional energy loss approach, have been limited to light hadrons [43], jets [44] and jet substructure [44, 45].

An important step toward generalizing such a unified description to heavy flavor is to include quark masses into SCET$_{\rm G}$. The SCET$_{\rm M}$ Lagrangian in the vacuum including quark masses was obtained in [46]. The introduction of heavy quark masses requires a specific power counting, where $m/p^+ \sim \lambda$ is of the order of the small power counting parameter in SCET. This is also consistent with the power counting for the dominant transverse momentum component of the Glauber gluon exchange $\sim (\lambda^2, \lambda^2, \lambda)$. Hence, to lowest order the new effective theory of heavy quark propagation in matter [47] SCET$_{\rm M,G}$ =SCET$_{\rm M}\otimes$SCET$_{\rm G}$.

The three splitting processes where the heavy quark mass plays a role are $Q \to Qg$, $Q \to gQ$ and $g \to Q\bar{Q}$. Going beyond the energy loss limit of soft gluon emission, a more careful consideration of parton splitting and deflection kinematics is necessary. We define the following transverse momentum

vectors

$$\mathbf{A}_\perp = \mathbf{k}_\perp,\ \mathbf{B}_\perp = \mathbf{k}_\perp + \mathbf{x}\mathbf{q}_\perp,\ \mathbf{C}_\perp = \mathbf{k}_\perp - (\mathbf{1}-\mathbf{x})\mathbf{q}_\perp,\ \mathbf{D}_\perp = \mathbf{k}_\perp - \mathbf{q}_\perp, \tag{8}$$

Here, x and $\mathbf{k}_\perp$ are the longitudinal momentum fraction and the transverse momentum of the emitted parton relative to the parent parton, respectively. $\mathbf{q}_\perp$ is the transverse momentum introduced by the Glauber gluon exchange. Interference phases read

$$\Omega_1 - \Omega_2 = \tfrac{\mathbf{B}_\perp^2+\nu^2}{p_0^+ x(1-x)},\ \Omega_1 - \Omega_3 = \tfrac{\mathbf{C}_\perp^2+\nu^2}{p_0^+ x(1-x)},\ \Omega_2 - \Omega_3 = \tfrac{\mathbf{C}_\perp^2-\mathbf{B}_\perp^2}{p_0^+ x(1-x)},$$
$$\Omega_4 = \tfrac{\mathbf{A}_\perp^2+\nu^2}{p_0^+ x(1-x)},\ \Omega_5 = \tfrac{\mathbf{A}_\perp^2-\mathbf{D}_\perp^2}{p_0^+ x(1-x)}\,. \tag{9}$$

The variable $\nu = x\,m\ \ (Q \to Qg)\,,\ \nu = (1-x)\,m\ \ (Q \to gQ)\,,\ \nu = m\ \ (g \to Q\bar{Q})$. Note that the way in which the "dead cone" [48] mass corrections enter in the interference phases and, as we shall see below, the propagators depends on the type of splitting function. The full medium induced splitting function for $Q \to Qg$ is given by

$$\begin{aligned}
&\left(\frac{dN^{\rm med}}{dxd^2\mathbf{k}_\perp}\right)_{Q\to Qg} = \frac{\alpha_s}{2\pi^2}C_F\int\frac{d\Delta z}{\lambda_g(z)}\int d^2\mathbf{q}_\perp\frac{1}{\sigma_{el}}\frac{d\sigma_{el}^{\rm med}}{d^2\mathbf{q}_\perp}\left\{\left(\frac{1+(1-x)^2}{x}\right)\left[\frac{\mathbf{B}_\perp}{\mathbf{B}_\perp^2+\nu^2}\right.\right.\\
&\times\left(\frac{\mathbf{B}_\perp}{\mathbf{B}_\perp^2+\nu^2}-\frac{\mathbf{C}_\perp}{\mathbf{C}_\perp^2+\nu^2}\right)(1-\cos[(\Omega_1-\Omega_2)\Delta z])+\frac{\mathbf{C}_\perp}{\mathbf{C}_\perp^2+\nu^2}\cdot\left(2\frac{\mathbf{C}_\perp}{\mathbf{C}_\perp^2+\nu^2}-\frac{\mathbf{A}_\perp}{\mathbf{A}_\perp^2+\nu^2}\right.\\
&\left.-\frac{\mathbf{B}_\perp}{\mathbf{B}_\perp^2+\nu^2}\right)(1-\cos[(\Omega_1-\Omega_3)\Delta z])+\frac{\mathbf{B}_\perp}{\mathbf{B}_\perp^2+\nu^2}\cdot\frac{\mathbf{C}_\perp}{\mathbf{C}_\perp^2+\nu^2}(1-\cos[(\Omega_2-\Omega_3)\Delta z])\\
&+\frac{\mathbf{A}_\perp}{\mathbf{A}_\perp^2+\nu^2}\cdot\left(\frac{\mathbf{D}_\perp}{\mathbf{D}_\perp^2+\nu^2}-\frac{\mathbf{A}_\perp}{\mathbf{A}_\perp^2+\nu^2}\right)(1-\cos[\Omega_4\Delta z])-\frac{\mathbf{A}_\perp}{\mathbf{A}_\perp^2+\nu^2}\cdot\frac{\mathbf{D}_\perp}{\mathbf{D}_\perp^2+\nu^2}(1-\cos[\Omega_5\Delta z])\\
&\left.+\frac{1}{N_c^2}\frac{\mathbf{B}_\perp}{\mathbf{B}_\perp^2+\nu^2}\cdot\left(\frac{\mathbf{A}_\perp}{\mathbf{A}_\perp^2+\nu^2}-\frac{\mathbf{B}_\perp}{\mathbf{B}_\perp^2+\nu^2}\right)(1-\cos[(\Omega_1-\Omega_2)\Delta z])\right]\\
&\left.+x^3m^2\left[\frac{1}{\mathbf{B}_\perp^2+\nu^2}\cdot\left(\frac{1}{\mathbf{B}_\perp^2+\nu^2}-\frac{1}{\mathbf{C}_\perp^2+\nu^2}\right)(1-\cos[(\Omega_1-\Omega_2)\Delta z])+\ \ldots\right]\right\}
\end{aligned}\tag{10}$$

where $\ldots$ indicate similar terms as in the first square bracket. The splitting function $Q \to gQ$ is given by symmetry and finally for the splitting function $g \to Q\bar{Q}$ is given by

$$\begin{aligned}
&\left(\frac{dN^{\rm med}}{dxd^2\mathbf{k}_\perp}\right)_{g\to Q\bar{Q}} = \frac{\alpha_s}{2\pi^2}T_R\int d\Delta z\frac{1}{\lambda_q(z)}\int d^2\mathbf{q}_\perp\frac{1}{\sigma_{el}}\frac{d\sigma_{el}^{\rm med}}{d^2\mathbf{q}_\perp}\left\{\left(x^2+(1-x)^2\right)\right.\\
&\times\left[2\,\frac{\mathbf{B}_\perp}{\mathbf{B}_\perp^2+\nu^2}\cdot\left(\frac{\mathbf{B}_\perp}{\mathbf{B}_\perp^2+\nu^2}-\frac{\mathbf{A}_\perp}{\mathbf{A}_\perp^2+\nu^2}\right)(1-\cos[(\Omega_1-\Omega_2)\Delta z])\right.\\
&+2\,\frac{\mathbf{C}_\perp}{\mathbf{C}_\perp^2+\nu^2}\cdot\left(\frac{\mathbf{C}_\perp}{\mathbf{C}_\perp^2+\nu^2}-\frac{\mathbf{A}_\perp}{\mathbf{A}_\perp^2+\nu^2}\right)(1-\cos[(\Omega_1-\Omega_3)\Delta z])+\frac{1}{N_c^2-1}\left(2\frac{\mathbf{B}_\perp}{\mathbf{B}_\perp^2+\nu^2}\right.\\
&\times\left(\frac{\mathbf{C}_\perp}{\mathbf{C}_\perp^2+\nu^2}-\frac{\mathbf{A}_\perp}{\mathbf{A}_\perp^2+\nu^2}\right)(1-\cos[(\Omega_1-\Omega_2)\Delta z])+2\,\frac{\mathbf{C}_\perp}{\mathbf{C}_\perp^2+\nu^2}\cdot\left(\frac{\mathbf{B}_\perp}{\mathbf{B}_\perp^2+\nu^2}-\frac{\mathbf{A}_\perp}{\mathbf{A}_\perp^2+\nu^2}\right)\\
&\times(1-\cos[(\Omega_1-\Omega_3)\Delta z])-2\,\frac{\mathbf{C}_\perp}{\mathbf{C}_\perp^2+\nu^2}\cdot\frac{\mathbf{B}_\perp}{\mathbf{B}_\perp^2+\nu^2}\cdot(1-\cos[(\Omega_2-\Omega_3)\Delta z])\\
&+2\,\frac{\mathbf{A}_\perp}{\mathbf{A}_\perp^2+\nu^2}\cdot\left(\frac{\mathbf{A}_\perp}{\mathbf{A}_\perp^2+\nu^2}-\frac{\mathbf{D}_\perp}{\mathbf{D}_\perp^2+\nu^2}\right)(1-\cos[\Omega_4\Delta z])\\
&\left.\left.+2\,\frac{\mathbf{A}_\perp}{\mathbf{A}_\perp^2+\nu^2}\cdot\frac{\mathbf{D}_\perp}{\mathbf{D}_\perp^2+\nu^2}(1-\cos[\Omega_5\Delta z])\right)\right]
\end{aligned}$$

$$+m^2\left[2\,\frac{1}{\mathbf{B}_\perp^2+\nu^2}\cdot\left(\frac{1}{\mathbf{B}_\perp^2+\nu^2}-\frac{1}{\mathbf{A}_\perp^2+\nu^2}\right)(1-\cos[(\Omega_1-\Omega_2)\Delta z])+\ldots\right]\right\}. \tag{11}$$

The results shown here emphasize the idea of separating the perturbative splitting processes induced by Glauber gluon interactions from the medium, which can be non-perturbative. As such, the above expressions are applicable for both QGP and cold nuclear matter but one has to take into account the different transport properties of these systems. Furthermore, effective parton masses generated by the medium regulate the transverse-momentum propagators and also figure in interference phases as $\mathbf{k^2}\to\mathbf{k^2}+\mathbf{m^2_{\rm eff}}$, where in the QGP $m^2_{\rm eff}\sim\mu_D^2$ (the Debye screening mass) and $m^2_{\rm eff}\sim m_\rho^2$ (a scale of low energy nuclear physics of order of the vector meson masses).

4.5.2 The soft gluon emission limit

The soft gluon emission limit, i.e. the limit when $x=k^+/p^+\ll 1$, is the only limit where a radiative energy loss interpretation of the general splitting processes described above can be given. It is easy to see that the $Q\to gQ$ and $g\to Q\bar{Q}$ splittings are formally suppressed. Taking the small-x limit in $Q\to Qg$ yields

$$\begin{aligned}x\left(\frac{dN^{\rm SGA}}{dxd^2\mathbf{k}_\perp}\right)_{Q\to Qg}&=\frac{\alpha_s}{\pi^2}C_F\int d\Delta z\frac{1}{\lambda_g(z)}\int d^2\mathbf{q}_\perp\frac{1}{\sigma_{el}}\frac{d\sigma_{el}^{\rm med}}{d^2\mathbf{q}_\perp}\\&\times\frac{2\mathbf{k}_\perp\cdot\mathbf{q}_\perp}{[\mathbf{k}_\perp^2+\mathbf{x^2m^2}][(\mathbf{k}_\perp-\mathbf{q}_\perp)^2+\mathbf{x^2m^2}]}\left[1-\cos\frac{(\mathbf{k}_\perp-\mathbf{q}_\perp)^2+\mathbf{x^2m^2}}{xp_0^+}\Delta z\right],\end{aligned} \tag{12}$$

a much simpler result.

The comparison of the full splitting kernels with the ressults of the soft gluon limit, and the comparison of massless and finite-mass partons, is given in Fig. 6. We show results for splitting functions averaged over the binary collision-distributed jet production in central Pb+Pb collisions at $\sqrt{s_{\rm NN}}=5.02$ TeV at the LHC in a gluon-dominated plasma. Note the pronounced differences between the massless and massive cases. It is also important to observe that in the energy region where mass effects are most important, the difference between the full splitting functions and the soft gluon approximation in the massless case are rather small, while in the massive case these are appreciable.

4.5.3 Effects of uncertainties in the heavy meson production mechanism

Traditionally, energy loss calculations have focused on a scenario where only heavy quarks fragment into heavy mesons. This leads to simple arguments about mass and color charge ordering of light-hadron, D-meson and B-meson suppression. The splitting functions above imply that both light partons and heavy quarks can fragment into heavy mesons. This will, of course, have implications for their expected quenching. It is important to identify the regions where the uncertainty due to the possibly different production mechanisms is minimal.

In p+p collisions a good description of heavy meson production can be achieved using the fragmentation functions of Refs. [49, 50, 51, 52]. The calculation combines the zero mass variable flavor number scheme [53, 54], and the $pp\to HX$ NLO framework [55, 56] yielding

$$\frac{d\sigma_{pp}^H}{dp_T d\eta}=\frac{2p_T}{s}\sum_{a,b,c}\int_{x_a^{\rm min}}^1\frac{dx_a}{x_a}f_a(x_a,\mu)\int_{x_b^{\rm min}}^1\frac{dx_b}{x_b}f_b(x_b,\mu)$$

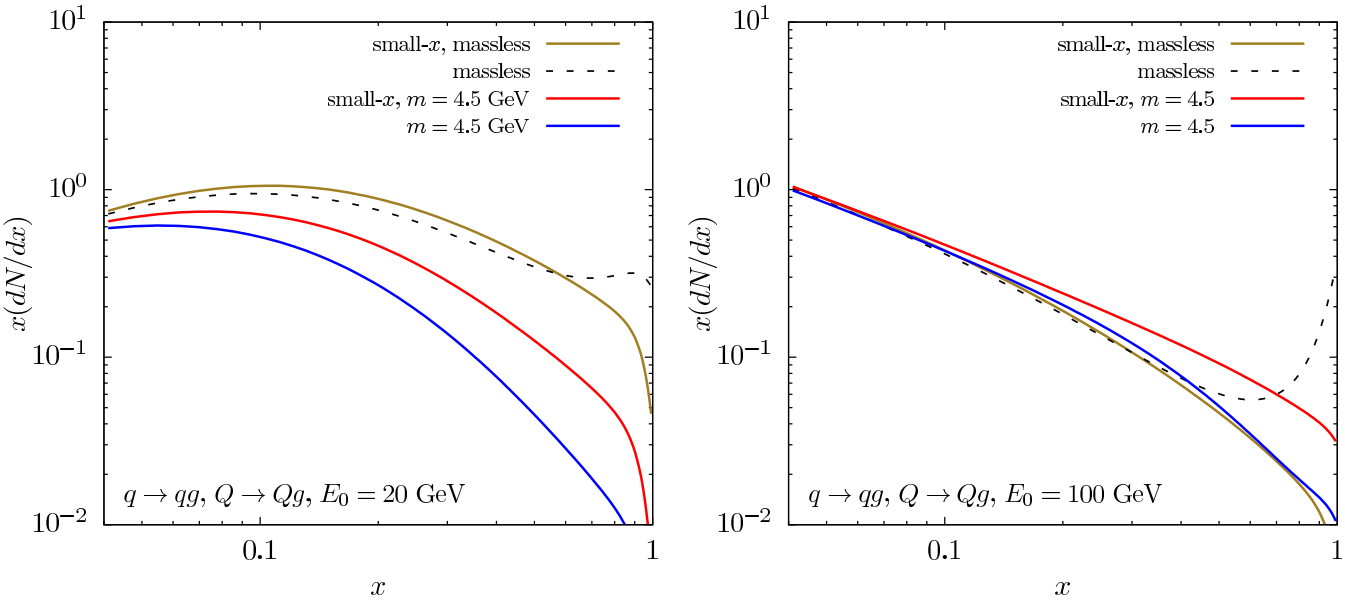

Figure 6: Comparison of the intensity spectra $x(dN/dx)$ for the heavy quark-to-quark splitting process. The massive results for the full splitting $Q \to Qg$ are in blue the corresponding small-x results are in red. We have choosen the mass $m_b = 4.5$ GeV. We also plot the massless results $q \to qg$ for both the full splitting in dashed black and the small-x limit in green. Left panel is for $E_0 = p_0^+/2 = 20$ GeV and right panel is for $E_0 = 100$ GeV.

$$\times \int_{z_c^{\min}}^1 \frac{dz_c}{z_c^2} \frac{d\hat{\sigma}_{ab}^c(\hat{s}, \hat{p}_T, \hat{\eta}, \mu)}{dvdz} D_c^H(z_c, \mu), \tag{13}$$

An example of D-meson production at the LHC is shown in the left panel of Fig. 7. The right panel of Fig. 7 shows the fractional contributions of heavy quark and gluon fragmentation to D mesons. Those contributions are approximately equal and the same is true for B mesons.

Going beyond the soft gluon approximation requires a new treatment of the medium-induced parton shower. Incorporating this contribution consistent with next-to-leading (NLO) calculation can be schematically expressed as

$$d\sigma_{\rm PbPb}^H = d\sigma_{pp}^{H,\rm NLO} + d\sigma_{\rm PbPb}^{H,\rm med}, \tag{14}$$

where $d\sigma_{pp}^{H,\rm NLO}$ is the NLO cross section in the vacuum, and $d\sigma_{\rm PbPb}^{H,\rm med} = \hat{\sigma}_i^{(0)} \otimes D_i^{H,\rm med}$ is the one-loop medium correction.

The suppresion of heavy mesons that originate from gluon fragmentation can be considerably stronger than the suppression of heavy mesons that originate form heavy quark fragmentation. The nuclear modification factors become equal only at very hight p_T, where the larger "energy loss" of gluons is offset by its softer fragmentation function. A practical way, however, of determining the region where the perturbative calculations can be used to probe the properties of the medium is to compare the $R_{AA}(p_T)$ from the energy loss and the full NLO calculation. Results are presented in Fig. 8. For D mesons the results are fairly comparable within uncertainties. For B mesons there is significant deviation below $p_T \sim 20$ GeV. At those transverse momenta collisional energy loss, described elsewhere in this document, and/or heavy meason dissociation [58, 59, 60] can play a role. However, it is important to realize that there is uncertainty in the absolute magnitude of the suppression based on medium-induced splitting/radiative processes that has not been discussed in the literature.

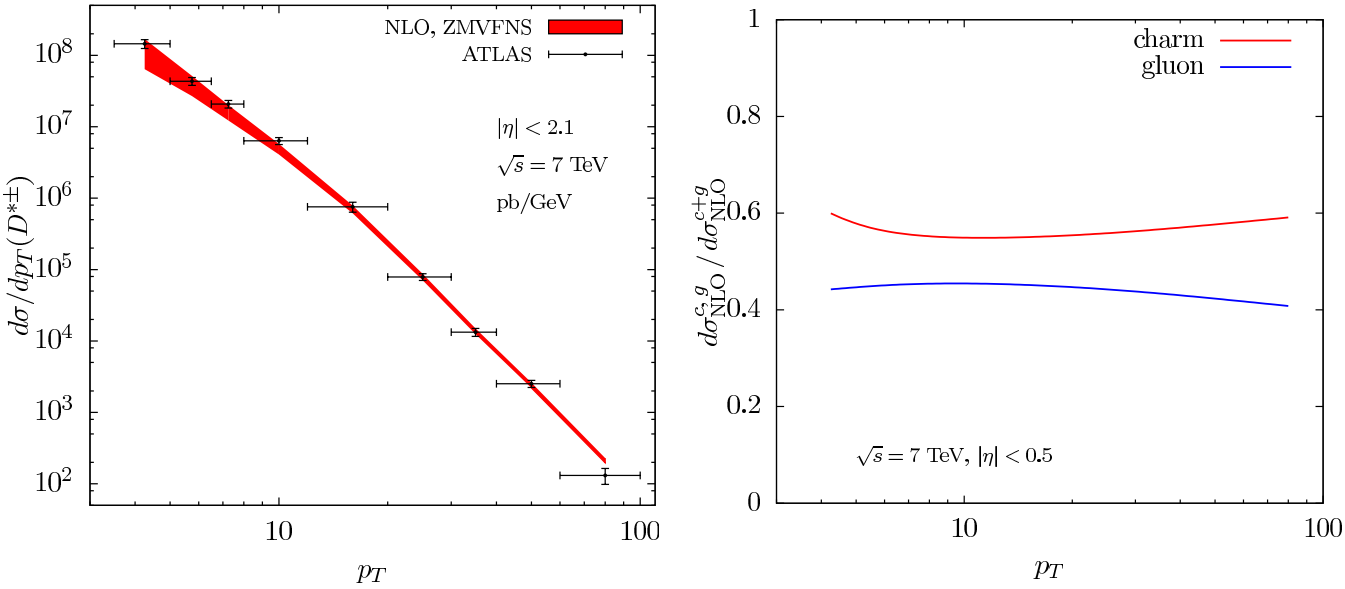

Figure 7: Left panel: differential cross sections for $pp \to D^{*\pm}X$ at $\sqrt{s} = 7$ TeV. Data is from ATLAS [57]. Right panel: the contribution of the heavy quark and gluon fragmentation processes to inclusive D-meson production at the LHC.

4.6 "Applicability Chart" in (p, T)

[**DRAFT: P. Gossiaux**];
Delimit possible transition regimes

5 Implementation of Heavy-Flavor Transport

5.1 Boltzmann vs. Langevin

[**DRAFT: V. Greco**];
figure of merit for m_Q/T;
applicability regimes depending on underlying bulk medium structure and quasi-particle approximation for charm and bottom;
"best" compromise of implementing Einstein relation (Guy: Langevin is not a good model at high p_T);
ways of estimating systematic uncertainties ... too conservative, so preference of readjusting B_1 (guideline)

5.2 Non-Locality in Radiative Energy Loss

Effective prescriptions; thermal field theory limit;
question of detailed balance, *i.e.*, $3 \to 2$ processes

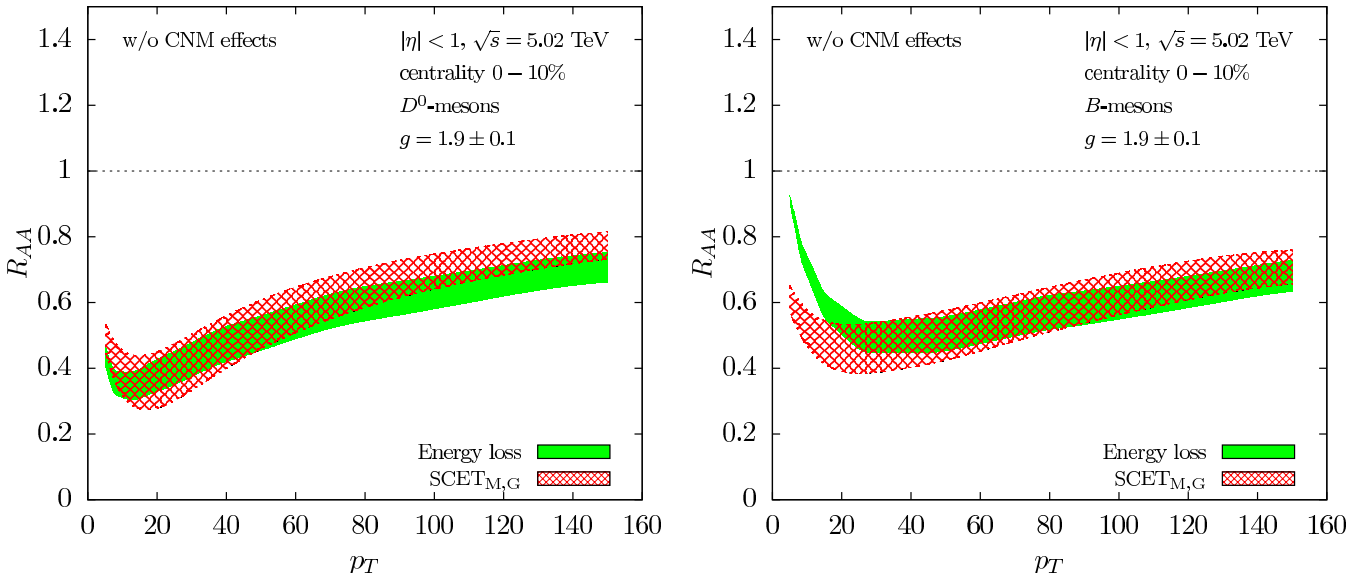

Figure 8: The nuclear modification factor R_{AA} for D^0 meson (left) and for B^+ meson (right) production as a function of the transverse momentum p_T. Result obtained within the traditional approach to energy loss are shown by a green band. Results based on SCET$_{\rm M,G}$ are shown by hatched red band.

6 Initial Heavy-Flavor Spectra

6.1 Parameterization for pp

[**DRAFT: A. Dainese, Y.J. Lee, F. Prino, C. Zaida**];
Compare initial HF spectra as used in existing transport calculations;
Provide standardized initial c-quark spectra fit to pp D-meson p_T spectra with standardized FF function **[Dainese,Lee,Prino,Zaida]**

6.2 Cold Nuclear Matter Effects

[**DRAFT: A. Dainese, Y.J. Lee, F. Prino, C. Zaida**];
EPS09 incl. uncertainty;
Cronin effect
[Dainese,Lee,Prino,Zaida]

7 Summary

Acknowledgments
EMMI RRTF; This work has been supported by *various funding agencies*

A Error Assessment

[**DRAFT: P. Gossiaux**];
possible method of uncertainty (de-)convolution:
Obs. = TransCoeff × BulkEvo × Hadroniz × ...
and then compensate systematic uncertainty into TC; possibly not generally feasible for all approaches

B Candid model description

critical assessment identifying areas of improvement

References

[1] H. Niemi, K. J. Eskola and R. Paatelainen, "Event-by-event fluctuations in a perturbative QCD + saturation + hydrodynamics model: Determining QCD matter shear viscosity in ultrarelativistic heavy-ion collisions," Phys. Rev. C **93**, no. 2, 024907 (2016)

[2] B. Svetitsky, "Diffusion of charmed quarks in the quark-gluon plasma," Phys. Rev. D **37**, 2484 (1988).

[3] A. Beraudo, "Dynamics of heavy flavor quarks in high energy nuclear collisions," Nucl. Phys. A **931**, 145 (2014)

[4] A. Andronic *et al.*, "Heavy-flavour and quarkonium production in the LHC era: from protonproton to heavy-ion collisions," Eur. Phys. J. C **76**, no. 3, 107 (2016)

[5] F. Prino and R. Rapp, "Open Heavy Flavor in QCD Matter and in Nuclear Collisions," J. Phys. G **43** (2016) no.9, 093002

[6] ExtreMe Matter Institute (EMMI) Rapid Reaction Task Force (RRTF) Meeting on *Extraction of heavy-flavor transport coefficients in QCD matter*, A. Andronic *et al.*, GSI Darmstadt (Germany), July 18-22 (2016); https://indico.gsi.de/conferenceDisplay.py?confId=5049

[7] http://www-alice.gsi.de/HQ_RRTF_2016/

[8] Z. w. Lin and D. Molnar, "Quark coalescence and elliptic flow of charm hadrons," Phys. Rev. C **68**, 044901 (2003)

[9] V. Greco, C. M. Ko and R. Rapp, "Quark coalescence for charmed mesons in ultrarelativistic heavy ion collisions," Phys. Lett. B **595** (2004) 202

[10] M. He, R. J. Fries and R. Rapp, "$\mathbf{D_s}$-Meson as Quantitative Probe of Diffusion and Hadronization in Nuclear Collisions," Phys. Rev. Lett. **110** (2013) 112301.

[11] P. Petreczky, Eur. Phys. J. **C62**, 85 (2009)

[12] P. Petreczky, P. Hegde and A. Velytsky [RBC-Bielefeld Collaboration], "Quark number fluctuations at high temperatures," PoS **LAT2009**, 159 (2009).

[13] P. Petreczky and D. Teaney, "Heavy quark diffusion from the lattice," Phys. Rev. D **73** (2006) 014508

[14] S. Caron-Huot, M. Laine and G. D. Moore, "A Way to estimate the heavy quark thermalization rate from the lattice," JHEP **0904**, 053 (2009)

[15] D. Banerjee, S. Datta, R. Gavai and P. Majumdar, "Heavy Quark Momentum Diffusion Coefficient from Lattice QCD," Phys. Rev. D **85** (2012) 014510.

[16] H. T. Ding, A. Francis, O. Kaczmarek, F. Karsch, H. Satz and W. Soeldner, "Charmonium properties in hot quenched lattice QCD," Phys. Rev. D **86** (2012) 014509.

[17] A. Francis, O. Kaczmarek, M. Laine, T. Neuhaus and H. Ohno, "Nonperturbative estimate of the heavy quark momentum diffusion coefficient," Phys. Rev. D **92** (2015) 116003.

[18] J. Casalderrey-Solana and D. Teaney, "Heavy quark diffusion in strongly coupled N=4 Yang-Mills," Phys. Rev. D **74** (2006) 085012.

[19] Y. Burnier, M. Laine, J. Langelage and L. Mether, "Colour-electric spectral function at next-to-leading order," JHEP **1008** (2010) 094

[20] S. Caron-Huot and G. D. Moore, "Heavy quark diffusion in QCD and N=4 SYM at next-to-leading order," JHEP **0802** (2008) 081

[21] S. Mukherjee, P. Petreczky and S. Sharma, "Charm degrees of freedom in the quark gluon plasma," Phys. Rev. D **93** (2016) 014502.

[22] A. Bazavov, F. Karsch, Y. Maezawa, S. Mukherjee and P. Petreczky, "In-medium modifications of open and hidden strange-charm mesons from spatial correlation functions," Phys. Rev. D **91** (2015) 054503.

[23] A. Bazavov *et al.*, "The melting and abundance of open charm hadrons," Phys. Lett. B **737** (2014) 210

[24] A. Bazavov *et al.*, "Quark number susceptibilities at high temperatures," Phys. Rev. D **88** (2013) no.9, 094021

[25] A. Bazavov *et al.* [HotQCD Collaboration], "Fluctuations and Correlations of net baryon number, electric charge, and strangeness: A comparison of lattice QCD results with the hadron resonance gas model," Phys. Rev. D **86** (2012) 034509

[26] H.-T. Ding, S. Mukherjee, H. Ohno, P. Petreczky and H.-P. Schadler, "Diagonal and off-diagonal quark number susceptibilities at high temperatures," Phys. Rev. D **92** (2015) no.7, 074043

[27] S. Borsanyi, Z. Fodor, S. D. Katz, S. Krieg, C. Ratti and K. Szabo, "Fluctuations of conserved charges at finite temperature from lattice QCD," JHEP **1201** (2012) 138

[28] R. Bellwied, S. Borsanyi, Z. Fodor, S. D. Katz, A. Pasztor, C. Ratti and K. K. Szabo, "Fluctuations and correlations in high temperature QCD," Phys. Rev. D **92** (2015) no.11, 114505

[29] G. Aarts, C. Allton, D. De Boni, S. Hands, B. Jger, C. Praki and J. I. Skullerud, "Finite Temperature Lattice QCD - Baryons in the Quark-Gluon Plasma," Acta Phys. Polon. Supp. **9** (2016) 441

[30] A. Mocsy, P. Petreczky and M. Strickland, "Quarkonia in the Quark Gluon Plasma," Int. J. Mod. Phys. A **28** (2013) 1340012

[31] A. Mocsy and P. Petreczky, "Can quarkonia survive deconfinement?," Phys. Rev. D **77** (2008) 014501

[32] F. Riek and R. Rapp, "Quarkonia and Heavy-Quark Relaxation Times in the Quark-Gluon Plasma," Phys. Rev. C **82** (2010) 035201

[33] H. van Hees, V. Greco and R. Rapp, "Heavy-quark probes of the quark-gluon plasma at RHIC," Phys. Rev. C **73** (2006) 034913

[34] A. Adare *et al.* [PHENIX Collaboration], "Energy Loss and Flow of Heavy Quarks in Au+Au Collisions at s(NN)**(1/2) = 200-GeV," Phys. Rev. Lett. **98** (2007) 172301

[35] B. B. Abelev *et al.* [ALICE Collaboration], "Azimuthal anisotropy of D meson production in Pb-Pb collisions at $\sqrt{s_{\rm NN}} = 2.76$ TeV," Phys. Rev. C **90** (2014) no.3, 034904

[36] L. Ravagli and R. Rapp, "Quark Coalescence based on a Transport Equation," Phys. Lett. B **655** (2007) 126 doi:10.1016/j.physletb.2007.07.043

[37] M. He, R. J. Fries and R. Rapp, "Heavy-Quark Diffusion and Hadronization in Quark-Gluon Plasma," Phys. Rev. C **86** (2012) 014903

[38] V. Greco, C. M. Ko and P. Levai, "Parton coalescence at RHIC," Phys. Rev. C **68** (2003) 034904

[39] A. Idilbi and A. Majumder, *Extending Soft-Collinear-Effective-Theory to describe hard jets in dense QCD media*, *Phys. Rev.* **D80** (2009) 054022

[40] G. Ovanesyan and I. Vitev, *An effective theory for jet propagation in dense QCD matter: jet broadening and medium-induced bremsstrahlung*, *JHEP* **06** (2011) 080

[41] G. Ovanesyan and I. Vitev, *Medium-induced parton splitting kernels from Soft Collinear Effective Theory with Glauber gluons*, *Phys. Lett.* **B706** (2012) 371–378

[42] G. Ovanesyan, F. Ringer, and I. Vitev, *Initial-state splitting kernels in cold nuclear matter*, *Phys. Lett.* **B760** (2016) 706–712

[43] Z.-B. Kang, R. Lashof-Regas, G. Ovanesyan, P. Saad, and I. Vitev, *Jet quenching phenomenology from soft-collinear effective theory with Glauber gluons*, *Phys. Rev. Lett.* **114** (2015), no. 9 092002

[44] Y.-T. Chien and I. Vitev, *Towards the understanding of jet shapes and cross sections in heavy ion collisions using soft-collinear effective theory*, *JHEP* **05** (2016) 023

[45] Y.-T. Chien and I. Vitev, *Probing the hardest branching of jets in heavy ion collisions*, `arXiv:1608.07283`.

[46] A. K. Leibovich, Z. Ligeti, and M. B. Wise, *Comment on quark masses in SCET*, *Phys. Lett.* **B564** (2003) 231–234

[47] Z.-B. Kang, F. Ringer, and I. Vitev, *Effective field theory approach to open heavy flavor production in heavy-ion collisions*, `arXiv:1610.02043`.

[48] Y. L. Dokshitzer and D. E. Kharzeev, *Heavy quark colorimetry of QCD matter*, *Phys. Lett.* **B519** (2001) 199–206

[49] T. Kneesch, B. A. Kniehl, G. Kramer, and I. Schienbein, *Charmed-meson fragmentation functions with finite-mass corrections*, *Nucl. Phys.* **B799** (2008) 34–59

[50] B. A. Kniehl, G. Kramer, I. Schienbein, and H. Spiesberger, *Open charm hadroproduction and the charm content of the proton*, *Phys. Rev.* **D79** (2009) 094009

[51] B. A. Kniehl, G. Kramer, I. Schienbein, and H. Spiesberger, *Inclusive photoproduction of D^{*+-} mesons at next-to-leading order in the General-Mass Variable-Flavor-Number Scheme*, *Eur. Phys. J.* **C62** (2009) 365–374

[52] B. A. Kniehl, G. Kramer, I. Schienbein, and H. Spiesberger, *Inclusive Charmed-Meson Production at the CERN LHC*, *Eur. Phys. J.* **C72** (2012) 2082

[53] J. C. Collins and W.-K. Tung, *Calculating Heavy Quark Distributions*, *Nucl. Phys.* **B278** (1986) 934

[54] T. P. Stavreva and J. F. Owens, *Direct Photon Production in Association With A Heavy Quark At Hadron Colliders*, *Phys. Rev.* **D79** (2009) 054017

[55] F. Aversa, P. Chiappetta, M. Greco, and J. P. Guillet, *QCD Corrections to Parton-Parton Scattering Processes*, *Nucl. Phys.* **B327** (1989) 105.

[56] B. Jager, A. Schafer, M. Stratmann, and W. Vogelsang, *Next-to-leading order QCD corrections to high p(T) pion production in longitudinally polarized pp collisions*, *Phys. Rev.* **D67** (2003) 054005

[57] **ATLAS** Collaboration, G. Aad et al., *Measurement of $D^{*\pm}$, $D^{\pm}$ and $D_s^{\pm}$ meson production cross sections in pp collisions at $\sqrt{s} = 7$ TeV with the ATLAS detector*, *Nucl. Phys.* **B907** (2016) 717–763

[58] A. Adil and I. Vitev, *Collisional dissociation of heavy mesons in dense QCD matter*, *Phys. Lett.* **B649** (2007) 139–146

[59] R. Sharma, I. Vitev, and B.-W. Zhang, *Light-cone wave function approach to open heavy flavor dynamics in QCD matter*, *Phys. Rev.* **C80** (2009) 054902

[60] R. Sharma and I. Vitev, *High transverse momentum quarkonium production and dissociation in heavy ion collisions*, *Phys. Rev.* **C87** (2013), no. 4 044905